Hindawi
International Journal of Aerospace Engineering
Volume 2022, Article ID 9391236, 15 pages
https://doi.org/10.1155/2022/9391236

Research Article

Robust Integrated Guidance and Control Design for Angle Penetration Attack of Multimissiles

Huan Zhou and Xin Zhao

Aviation Engineering School, Air Force Engineering University, Xi'an, China

Correspondence should be addressed to Xin Zhao; 2182597520@qq.com

Received 14 January 2022; Revised 5 May 2022; Accepted 9 May 2022; Published 20 May 2022

Academic Editor: Miaomiao Wang

Angle penetration attack ability plays a more and more important role for missiles in modern warfare, and the traditional separate guidance and control system design problem is the key to restrict the improvement of time-sensitive attack and cooperative attack ability of multimissiles. Firstly, the deviation control strategy of line-of-sight angle and attack angle is put forward in this paper, and the integrated guidance and control system model with impact angle constraint is established, according to the characteristics of angle penetration attack. Then, an integrated guidance and control controller for angle penetration attack is designed by using adaptive dynamic surface control, with the dynamic constraints, nonlinear input saturation, and terminal line-of-sight and attack angle constraints concerned. In order to ensure the robustness of the system, nonlinear disturbance observers are introduced to estimate the uncertainty of the system model. Finally, the stability of the integrated design method is proven based on the Lyapunov theory. Simulation results verify the effectiveness of the integrated guidance and control design method proposed in this paper in multimissile angle penetration attack.

1. Introduction

Multimissile angle penetration attack is a combat mode in which multiple missiles strike the target at different terminal impact angles. It plays an irreplaceable important role in modern war by meeting a variety of specific combat requirements to destroy the enemy target to the greatest extent [1, 2]. In the process of multimissile attack mission, the guidance and control system is the key to realize cooperative precision attack, and the performance of the system will ultimately determine the operational effectiveness of the missile.

The traditional design scheme of the missile guidance and control system is to separate the guidance system from the control system and then design two systems separately [3, 4]. The core of the traditional separate guidance and control design method lies in the design of guidance law. The designed system gives the desired control command through the guidance law and then executes the control command by the flight control system, in order to control the missile to maintain a stable flight attitude and perform the task of attacking battlefield targets.

In the design of attack time cooperation, Jeon et al. [5] proposed an attack time control guidance law for antiship missiles based on the idea of optimal control. Kumar and Ghose [6] set the error term between the preset attack time and the remaining attack time, added it to the proportional guidance law, and designed a new guidance law through the sliding mode control method to ensure that the preset attack time constraints are met. Both the attack time control guidance law and the sliding mode guidance law do not fully consider the interaction and cooperation in the flight process of missiles; therefore, Ref. [7, 8] designed a two-layer structure of cooperative guidance framework and cooperative proportional guidance law. In the process of combat flight, missiles share the remaining attack time information through online data link and adjust its own flight state in real time to achieve the coordination of the final attack time. In terms of the impact angle cooperation, Harl and Balakrishnan [9] designed a cooperative guidance law with attack time and attack angle constraints based on sliding mode control and comprehensively adopted line-of-sight rate adjustment technology and second-order sliding mode

method to meet the attack time and attack angle constraints. Jung and Kim [10] designed the offset proportional guidance law by using the backstepping control method, in which the offset term comprehensively considered the attack time error and attack angle error.

The traditional guidance and control system design scheme can realize the cooperative attack flight guidance and control of multimissiles by designing the cooperative guidance law. However, the time constant of the guidance loop becomes smaller and the bandwidth becomes larger with the gradual reduction of the relative distance between the missile and the target. At this time, the assumption of frequency spectrum separation will no longer be tenable; the traditional separation design scheme will lead to the problems that seriously restrict the missile combat capability, such as sharp performance degradation, large miss distance, and flight instability. The integrated guidance and control (IGC) scheme is an effective way to solve this problem [11, 12].

The research on the IGC mainly focuses on the control of a single aircraft/missile, mainly including optimal control method [13], backstepping control method [14], sliding mode control method [15], trajectory linearization control method [16], and dynamic surface control method [17]. It is extremely difficult to apply the IGC to the cooperative control of multimissiles. In particular for the angle penetration attack, the guidance and control system should not only ensure that the terminal impact angle attitude of each missile meets a specific constraint requirement but also minimize the attack angle of missiles when intercepting the target. At the same time, the existing cooperative IGC design lacks full consideration and in-depth research on the problems of system stability and robustness caused by the nonlinearity and time variability of the missile itself, the perturbation of missile aerodynamic parameters, and the limitation of input saturation.

The dynamic surface control method is first proposed by Swaroop et al. [17], to overcome the problem of "item explosion" in backstepping control method and sliding mode control method. Its basic idea is to add a first-order low-pass filter between the designs of the two-step control laws of the original backstepping control, so as to avoid the direct differentiation of some nonlinear signals in the next design [18]. The deficiency of the dynamic surface control method is how to improve its adaptive and robust performance in complex system environment.

The IGC system modelling of multimissile angle penetration attack is a typical nonlinear problem, which is very difficult to control [19, 20]. The contribution of this work is to design a robust IGC method to increase the adaptive and robust performance of the DSC when the missile system itself has control input saturation, and there is nonlinearly parameterized no-matching uncertainty in the system. Meanwhile, the cooperative problem of the IGC control is effectively processed.

Aimed at the problem of multimissile cooperative attack on one stationary target, a three-channel independent decoupling model of the integrated guidance and control (IGC) system with impact angle constraint is established firstly, according to the requirements of angle penetration attack. On this basis, a robust IGC control method for angle penetration attack is designed by using adaptive dynamic surface (DSC) control and nonlinear disturbance observer (NDO) technology. Finally, simulation experiments are carried out, in order to verify the effectiveness of the IGC design method proposed for multimissile angle penetration attack.

2. IGC System Modelling of Multimissile Angle Penetration Attack

The flight control system model of a single missile and the three-channel independent decoupling model of the IGC system are shown in document [21, 22]. This section mainly establishes the cooperative IGC system model of multimissiles with impact angle constraints according to the relative motion relationship for angle penetration attack between multimissiles and the target. In order to ensure the coordination of the flight state of multiple missiles, the photoelectric infrared detector can obtain the corresponding distance and angle information, but the price is expensive. In practice, the small radar or radio spectrum detection equipment can be put on every missile for a distributed control system, or the data of each missile comes from the central data link.

2.1. Relative Motion Relationship between Multimissiles and Targets. At the end of multimissile cooperative attack, assuming that N missiles attack one target and the target is stationary, the relative motion relationship between each missile and the target in the three-dimensional environment can be decomposed into independent relative motions in the longitudinal and lateral planes. The relative motion relationships in the two planes are shown in Figure 1(a) and 1(b), respectively.

In Figure 1, all quantities including subscripts y, z represent the components of missile and target related parameters in the longitudinal plane and lateral plane, respectively, where $R_{i,y}, R_{i,z}$ is the relative distance between the i-th missile and the target. By omitting the subscript i for convenience, V_{uy}, V_{uz} and V_{ty}, V_{tz} represent the speed of the i-th missile and the target, respectively; $\varphi_{uy}, \varphi_{uz}$ represent the included angle between the velocity vector of the i-th missile and the reference plane, that is, the track inclination and track deflection angle of the missile; $\varphi_{ty}, \varphi_{tz}$ are the angle between the target velocity vector and the reference plane, that is, the track inclination and track deflection angle of the target; $\varphi_{ry}, \varphi_{rz}$ are the line-of-sight (LOS) angle between the i-th missile and the target.

For the longitudinal plane pitch channel, the relative motion equation between the i-th missile and the target can be obtained from Figure 1(a):

$$\begin{cases} \dot{R}_y = -V_{uy} \cos\left(\varphi_{ry} - \varphi_{uy}\right), \\ R_y \dot{\varphi}_{ry} = V_{uy} \sin\left(\varphi_{ry} - \varphi_{uy}\right). \end{cases} \tag{1}$$

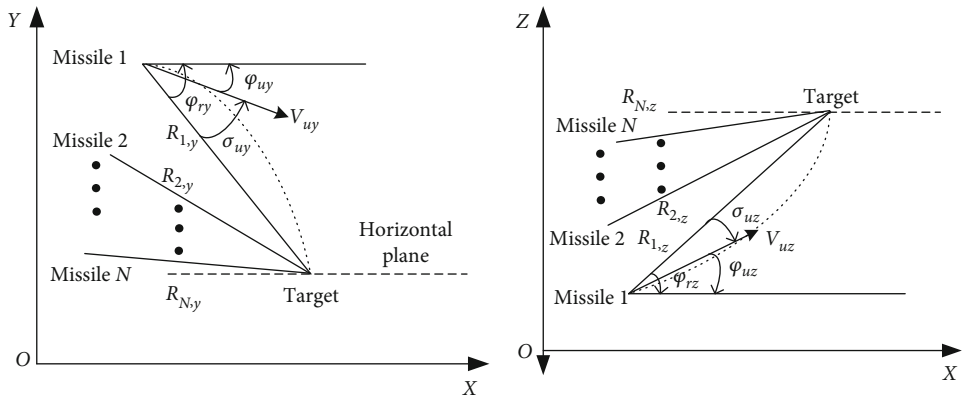

(a) Relative motion in the longitudinal plane (b) Relative motion in the lateral plane

Figure 1: Relative motion relationship between N missiles and one target.

By differentiating on both sides of equation (1), we get

$$\ddot{\varphi}_{ry} = \left[\frac{\dot{V}_{uy}}{V_{uy}} - \frac{2\dot{R}_y}{R_y}\right]\dot{\varphi}_{ry} + \frac{\dot{R}_y}{R_y}\dot{\varphi}_{uy}. \tag{2}$$

On the basis of Ref. [18], by adding the track inclination of the missile to the pitch channel subsystem, the pitch channel subsystem of the missile becomes

$$\begin{cases} \dot{\theta} = \dfrac{qSc_y^{\alpha} + P}{mV}\alpha + \Delta\theta, \\ \dot{\alpha} = \omega_z - \dfrac{qSc_y^{\alpha} + P}{mV}\alpha + \Delta\alpha, \\ \dot{\omega}_z = \dfrac{qSL}{J_z}\left(m_z^{\alpha}\alpha + m_z^{\delta_z}\delta_z + m_z^{\omega_z}\omega_z\right) + \Delta\omega_z, \end{cases} \tag{3}$$

where θ, α, w_z represent the track inclination, attack angle, and pitch angle rate of the missile, respectively, and $\Delta\theta, \Delta\alpha, \Delta\omega_z$ represent the corresponding unknown bounded uncertainty. The physical quantities represented by other parameters are shown in Ref. [18].

Combining equations (2) and (3), the following can be obtained:

$$\ddot{\varphi}_{ry} = \left[\frac{\dot{V}_{uy}}{V_{uy}} - \frac{2\dot{R}_y}{R_y}\right]\dot{\varphi}_{ry} + \frac{\left(qSc_y^{\alpha} + P\right)\dot{R}_y}{mV_{uy}R_y}\alpha + \Delta\varphi_{ry}. \tag{4}$$

Similarly, for the lateral plane yaw channel, the relative motion equation between the i-th missile and the target can be obtained from Figure 1(b):

$$\begin{cases} \dot{R}_z = -V_{uz}\cos\left(\varphi_{rz} - \varphi_{uz}\right), \\ R_z\dot{\varphi}_{rz} = V_{uz}\sin\left(\varphi_{rz} - \varphi_{uz}\right). \end{cases} \tag{5}$$

By differentiating on both sides of equation (5), we get

$$\ddot{\varphi}_{rz} = \left[\frac{\dot{V}_{uz}}{V_{uz}} - \frac{2\dot{R}_z}{R_z}\right]\dot{\varphi}_{rz} + \frac{\dot{R}_z}{R_z}\dot{\varphi}_{uz}. \tag{6}$$

On the basis of Ref. [18], by adding the track deflection angle of the missile to the yaw channel subsystem, the yaw channel subsystem of the missile becomes

$$\begin{cases} \dot{\psi} = -\dfrac{qSc_z^{\beta} - P}{mV}\beta + \Delta\psi, \\ \dot{\beta} = \omega_y + \dfrac{qSc_z^{\beta} - P}{mV}\beta + \Delta\beta, \\ \dot{\omega}_y = \dfrac{qSL}{J_y}\left(m_y^{\beta}\beta + m_y^{\delta_y}\delta_y + m_y^{\omega_y}\omega_y\right) + \Delta\omega_y, \end{cases} \tag{7}$$

where ψ, β, w_y represent the track yaw angle, sideslip angle, and yaw angle rate of the missile, respectively, and $\Delta\psi, \Delta\beta, \Delta\omega_y$ represent the corresponding unknown bounded uncertainty. The physical quantities represented by other parameters are shown in Ref. [18].

Since $\varphi_{uz} = \psi$, combining equations (6) and (7), the following can be obtained:

$$\ddot{\varphi}_{rz} = \left[\frac{\dot{V}_{uz}}{V_{uz}} - \frac{2\dot{R}_z}{R_z}\right]\dot{\varphi}_{rz} - \frac{\left(qSc_z^{\beta} - P\right)\dot{R}_z}{mV_{uz}R_z}\beta + \Delta\varphi_{rz}. \tag{8}$$

Therefore, equations (4) and (8) describe the differential expressions of the line-of-sight angle rate of the i-th missile and target in the longitudinal plane and lateral plane, respectively.

2.2. Three-Channel Independent Decoupling Model of the IGC System with Impact Angle Constraint. Through the analysis of the relative motion relationship between the missile and the target, the desired impact angles of the longitudinal plane and the lateral plane are noted as φ_{ry}^{d} and φ_{rz}^{d},

respectively, and the relationship between the current line-of-sight angle, the desired line-of-sight angle, the line-of-sight angle rate, and other state variables is established. The multimissile angle penetration attack is transformed into the problem of line-of-sight angle deviation and attack angle control.

Let the error between the current and the desired line-of-sight angle in the longitudinal plane and the lateral plane be, respectively,

$$\varphi_{ry}^{e} = \varphi_{ry} - \varphi_{ry}^{d}, \tag{9}$$

$$\varphi_{rz}^{e} = \varphi_{rz} - \varphi_{rz}^{d}. \tag{10}$$

By calculating the first derivative and the second derivative on both sides of equations (9) and (10), respectively, it can be seen that

$$\dot{\varphi}_{ry}^{e} = \dot{\varphi}_{ry}, \tag{11}$$

$$\ddot{\varphi}_{ry}^{e} = \ddot{\varphi}_{ry}, \tag{12}$$

$$\dot{\varphi}_{rz}^{e} = \dot{\varphi}_{rz}, \tag{13}$$

$$\ddot{\varphi}_{rz}^{e} = \ddot{\varphi}_{rz}. \tag{14}$$

According to equations (3), (4), (9), (11), and (12), by taking $[\varphi_{ry}^{e} \dot{\varphi}_{ry}^{e} \alpha \omega_z]^T$ as state variables, the subsystem model of the IGC pitch channel of the missile with impact angle constraint can be obtained as

$$\begin{cases} \dot{\varphi}_{ry}^{e} = \dot{\varphi}_{ry}^{e}, \\ \ddot{\varphi}_{ry}^{e} = \left[\dfrac{\dot{V}_{uy}}{V_{uy}} - \dfrac{2\dot{R}_y}{R_y}\right]\dot{\varphi}_{ry}^{e} + \dfrac{\left(qSc_y^{\alpha} + P\right)\dot{R}_y}{mV_{uy}R_y}\alpha + \Delta\varphi_{ry}, \\ \dot{\alpha} = \omega_z - \dfrac{qSc_y^{\alpha} + P}{mV}\alpha + \Delta\alpha, \\ \dot{\omega}_z = \dfrac{qSL}{J_z}\left(m_z^{\alpha}\alpha + m_z^{\delta_z}\delta_z + m_z^{\omega_z}\omega_z\right) + \Delta\omega_z. \end{cases} \tag{15}$$

Similarly, according to equations (7), (8), (10), (13), and (14), by taking $[\varphi_{rz}^{e} \dot{\varphi}_{rz}^{e} \beta \omega_y]^T$ as state variables, the subsystem model of the IGC yaw channel of the missile with impact angle constraint can be obtained as

$$\begin{cases} \dot{\varphi}_{rz}^{e} = \dot{\varphi}_{rz}^{e}, \\ \ddot{\varphi}_{rz}^{e} = \left[\dfrac{\dot{V}_{uz}}{V_{uz}} - \dfrac{2\dot{R}_z}{R_z}\right]\dot{\varphi}_{rz} - \dfrac{\left(qSc_z^{\beta} - P\right)\dot{R}_z}{mV_{uz}R_z}\beta + \Delta\varphi_{rz}, \\ \dot{\beta} = \omega_y + \dfrac{qSc_z^{\beta} - P}{mV}\beta + \Delta\beta, \\ \dot{\omega}_y = \dfrac{qSL}{J_y}\left(m_y^{\beta}\beta + m_y^{\delta_y}\delta_y + m_y^{\omega_y}\omega_y\right) + \Delta\omega_y. \end{cases} \tag{16}$$

Continue to take $[\gamma \omega_x]^T$ as state variables, and the subsystem model of the IGC roll channel of the missile with impact angle constraint can be obtained as

$$\begin{cases} \dot{\gamma} = \omega_x + \Delta\gamma, \\ \dot{\omega}_x = \dfrac{qSL}{J_x}m_x^{\delta_x}\delta_x + \Delta\omega_x. \end{cases} \tag{17}$$

To sum up, equations (15), (16), and (17) constitute the IGC three-channel independent decoupling system model of the missile with impact angle constraint.

3. Robust IGC Control Method for Angle Penetration Attack

The difference between the cooperative IGC model obtained above and the single IGC model described in Ref. [18] is that the single IGC model is a single-output linear time-varying system, while the cooperative IGC model is a multioutput linear time-varying system. At the same time, the missile angle penetration attack not only needs to meet the impact angle constraint but also needs to minimize the attack angle when completing the target attack. Therefore, by taking the subsystem model of the IGC pitch channel in the longitudinal plane as an example, a cooperative robust IGC control method based on the adaptive dynamic surface and nonlinear disturbance observer is designed.

Because the missile needs to meet the requirements of angle penetration attack, the motion of missiles will become more complex, compared with the precise attack flight process of a single missile. At this time, the control limitation of each rudder deflection angle of the missile needs to be considered.

Note the elevator yaw control limit as

$$|\delta_z| \le \delta_{z_{\max}}, \tag{18}$$

where $\delta_{z_{\max}} > 0$.

Define the actual rudder deflection angle of elevator as $\text{real}(\delta_z)$; then,

$$\text{real}(\delta_z) = \begin{cases} \delta_{z_{\max}}, \delta_z \geq \delta_{z_{\max}}, \\ \delta_z, \\ \delta_{z_{\max}}, \delta_z \leq -\delta_{z_{\max}}. \end{cases} \tag{19}$$

Let the state variables $x_1' = \varphi_{rz}^e$, $x_2' = \dot{\varphi}_{rz}^e$, $x_3' = \alpha$, and $x_4' = \omega_z$ and the control variable $u = \delta_z$ and $\Delta\varphi_{ry}, \Delta\alpha, \Delta\omega_z$ be recorded as $d_{\varphi_{ry}}, d_\alpha, d_{\omega_z}$, respectively; then, equation (15) can be rewritten into a general state space expression:

$$\begin{cases} \dot{x}_1' = f_1' + g_1' x_2', \\ \dot{x}_2' = f_2' + g_2' x_3' + d_{\varphi_{ry}}, \\ \dot{x}_3' = f_3' + g_3' x_4' + d_\alpha, \\ \dot{x}_4' = f_4' + g_4' \text{real}(\delta_z) + d_{\omega_z}, \end{cases} \tag{20}$$

where

$$\begin{bmatrix} f_1' \\ f_2' \\ f_3' \\ f_4' \end{bmatrix} = \begin{bmatrix} 0 \\ \left[\dfrac{\dot{V}_{uy}}{V_{uy}} - \dfrac{2\dot{R}_y}{R_y}\right]\dot{\varphi}_{ry}^e \\ -\dfrac{qSc_y^\alpha + P}{mV}\alpha \\ \dfrac{qSL}{J_z}(m_z^\alpha \alpha + m_z^{\omega_z}\omega_z) \end{bmatrix}; \begin{bmatrix} g_1' \\ g_2' \\ g_3' \\ g_4' \end{bmatrix} = \begin{bmatrix} 1 \\ \dfrac{\left(qSc_y^\alpha + P\right)\dot{R}_y}{mV_{uy}R_y} \\ 1 \\ \dfrac{qSLm_z^{\delta_z}}{J_z} \end{bmatrix}. \tag{21}$$

3.1. Robust IGC Controller Based on the Adaptive Dynamic Surface. For the IGC system model shown in equation (20), which contains unknown uncertainty and has control input constraints, the control goal is to design the controller to make the terminal line-of-sight angle between each missile and the target meet the desired impact angle requirements and ensure that the line-of-sight angle rate tends to zero and meet the requirements of low miss distance.

Before designing the control law, make the following assumptions.

Assumption 1. The system (20) is BIBO stable.

To compensate for the impact of input saturation, the following auxiliary subsystems are established:

$$\begin{cases} \dot{\xi}_1' = -h_1'\xi_1' + \xi_2', \xi_1'(0) = 0, \\ \dot{\xi}_2' = -h_2'\xi_2' + \xi_3', \xi_2'(0) = 0, \\ \dot{\xi}_3' = -h_3'\xi_3' + \xi_4', \xi_3'(0) = 0, \\ \dot{\xi}_4' = -h_4'\xi_4' + g_4'\Delta\delta_z, \xi_4'(0) = 0, \end{cases} \tag{22}$$

where $h_i' > 0 (i = 1, 2, 3, 4)$ and $\Delta\delta_z = \text{real}(\delta_z) - \delta_z$.

The design steps of the dynamic surface are as follows.

Step 1. Define the first dynamic face as

$$s_1' = x_1' - \xi_1'. \tag{23}$$

By deriving from both sides of equation (23) and combining the first equation in equation (20), the following can be obtained:

$$\dot{s}_1' = f_1' + g_1' x_2' + h_1'\xi_1' - \xi_2', \tag{24}$$

where x_2' is selected as the virtual control variable and designed as

$$x_{2c}' = \frac{-f_1' - k_1' s_1' - h_1'\xi_1' + \xi_2'}{g_1'}, \tag{25}$$

where k_1' is the constant to be set, and it meets that $k_1' > 0$. Since $g_1' = 1 \neq 0$, x_{2c}' is always nonsingular.

x_{2c}' is transmitted through the following first-order filter:

$$\tau_2'\dot{x}_{2d}' + x_{2d}' = x_{2c}', x_{2d}'(0) = x_{2c}'(0), \tag{26}$$

where τ_2' is the time constant of the filter.

Step 2. Define the second dynamic face as

$$s_2' = x_2' - x_{2d}' - \xi_2'. \tag{27}$$

By deriving from both sides of equation (27) and combining the second equation in equation (20), the following can be obtained:

$$\dot{s}_2' = f_2' + g_2' x_3' + d_{\varphi_{ry}} - \dot{x}_{2d}' + h_2'\xi_2' - \xi_3', \tag{28}$$

where x_3' is selected as the virtual control variable and designed as

$$x_{3c}' = \frac{-f_2' - k_2' s_2' - \widehat{d}_{\varphi_{ry}} + \dot{x}_{2d}' - h_2'\xi_2' + \xi_3'}{g_2'}, \tag{29}$$

where k_2' is the constant to be set, and it meets that $k_2' > 0$; $\widehat{d}_{\varphi_{ry}}$ is the estimation of $d_{\varphi_{ry}}$, that is, the output of the subsequently designed nonlinear disturbance observer (NDO). Since $g_2' = (qSc_y^\alpha + P)\dot{R}_y/(mV_{uy}R_y) \neq 0$, x_{3c}' is always nonsingular.

Similar to x_{2c}', x_{3c}' is transmitted through the following first-order filter:

$$\tau_3'\dot{x}_{3d}' + x_{3d}' = x_{3c}', x_{3d}'(0) = x_{3c}'(0), \tag{30}$$

where τ_3' is the time constant of the filter.

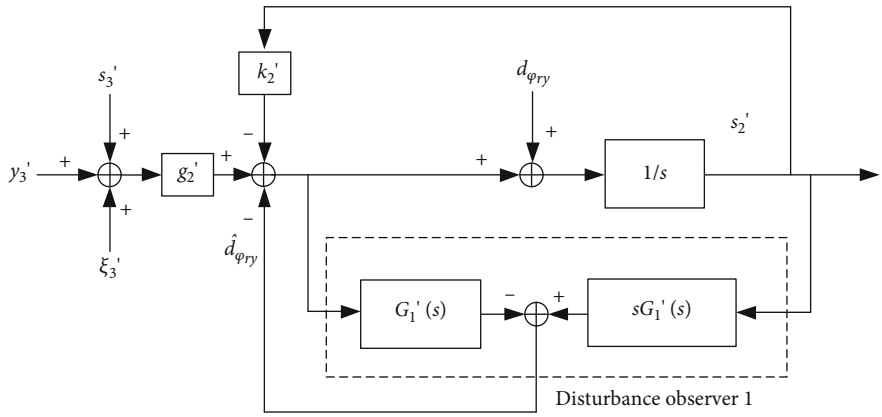

Figure 2: Disturbance observer for estimating $d_{\varphi_{ry}}$.

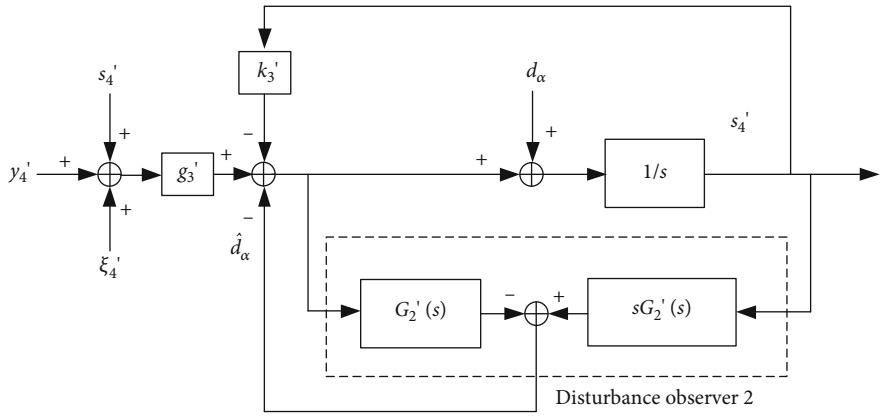

Figure 3: Disturbance observer for estimating d_α.

Step 3. Define the second dynamic face as

$$s_3' = x_3' - x_{3d}' - \xi_3'. \tag{31}$$

By deriving from both sides of equation (31) and combining the third equation in equation (20), the following can be obtained:

$$\dot{s}_3' = f_3' + g_3' x_4' + d_\alpha - \dot{x}_{3d}' + h_3' \xi_3' - \xi_4', \tag{32}$$

where x_4' is selected as the virtual control variable and designed as

$$x_{4c}' = \frac{-f_3' - k_3' s_3' - \widehat{d}_\alpha + \dot{x}_{3d}' - h_3' \xi_3' + \xi_4'}{g_3'}, \tag{33}$$

where k_3' is the constant to be set, and it meets that $k_3' > 0$; similar to $\widehat{d}_{\varphi_{ry}}$, $\widehat{d}_\alpha$ is the estimation of d_α, that is, the output of the subsequently designed nonlinear disturbance observer (NDO). Since $g_3' = 1 \neq 0$, x_{4c}' is always nonsingular.

Similar to x_{2c}' and x_{3c}', x_{4c}' is transmitted through the following first-order filter:

$$\tau_4' \dot{x}_{4d}' + x_{4d}' = x_{4c}', x_{4d}'(0) = x_{4c}'(0), \tag{34}$$

where τ_4' is the time constant of the filter.

Step 4. Define the second dynamic face as

$$s_4' = x_4' - x_{4d}' - \xi_4'. \tag{35}$$

By deriving from both sides of equation (35) and combining the fourth equation in equation (20), the following can be obtained:

$$\begin{aligned} \dot{s}_4' &= f_4' + g_4' (\text{real}(\delta_z) - \Delta\delta_z) + d_{\omega_z} - \dot{x}_{4d}' + h_4' \xi_4' \\ &= f_4' + g_4' \delta_z + d_{\omega_z} - \dot{x}_{4d}' + h_4' \xi_4'. \end{aligned} \tag{36}$$

Then, the actual control input is designed as

$$\delta_z = \frac{-f_4' - k_4' s_4' - \widehat{d}_{\omega_z} + \dot{x}_{4d}' - h_4' \xi_4'}{g_4'}, \tag{37}$$

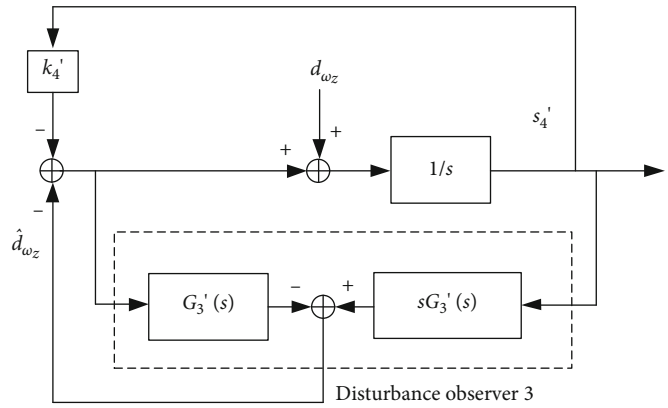

Figure 4: Disturbance observer for estimating d_{ω_z}.

1: For the IGC system mode by Equation (20), define auxiliary subsystems by Equation (22);
2: Design the first dynamic surface by Equation (23);
3: Design the second dynamic surface by Equation (27);
4: Design the third dynamic surface by Equation (31);
5: Design the fourth dynamic surface by Equation (35);
6: Design the first NDO to estimate $d_{\varphi_{ry}}$ by Figure 2;
7: Design the second NDO to estimate d_α by Figure 3;
8: Design the third NDO to estimate d_{ω_z} by Figure 4;
9: The controller work steps are completed.

Pseudocode 1: Controller work steps: robust integrated guidance and control design.

where $k_4{}'$ is the constant to be set, and it meets that $k_4{}' > 0$; similar to $\widehat{d}_{\varphi_{ry}}$ and $\widehat{d}_\alpha$, $\widehat{d}_{\omega_z}$ is the estimation of d_{ω_z}, that is, the output of the subsequently designed nonlinear disturbance observer (NDO). Since $g_4{}' = qSLm_z^{\delta_z}/J_z \neq 0$, δ_z is always nonsingular.

3.2. Nonlinear Disturbance Observer to Dealing with Uncertainty. In this section, three disturbance observers are designed to estimate the uncertainty $d_{\varphi_{ry}}, d_\alpha, d_{\omega_z}$, respectively, in order to enhance robustness of the IGC system.

According to equation (30), the error between filter output and input is defined as

$$y_3{}' = x_{3d}{}' - x_{3c}{}'. \tag{38}$$

Combining equations (31), (38), and (29), we can obtain

$$x_3{}' = s_3{}' + x_{3d}{}' + \xi_3{}' = s_3{}' + y_3{}' + x_{3c}{}' + \xi_3{}' = s_3{}' + y_3{}' + \frac{-f_2{}' - k_2{}' s_2{}' - \widehat{d}_{\varphi_{ry}} + \dot{x}_{2d}{}' - h_2\xi_2{}' + \xi_3{}'}{g_2{}'} + \xi_3{}'. \tag{39}$$

Substituting equation (39) into (27), we get

$$\dot{s}_2{}' = -k_2{}' s_2{}' + g_2{}' s_3{}' + g_2{}' y_3{}' + g_2{}' \xi_3{}' - \widehat{d}_{\varphi_{ry}} + d_{\varphi_{ry}}. \tag{40}$$

Therefore, according to the design steps of nonlinear disturbance observer in Ref. [18], the observer designed in this section for estimating $d_{\varphi_{ry}}$ is shown in Figure 2.

In Figure 2, the expression of low-pass filter $G_1{}'(s)$ is

$$G_1{}'(s) = \frac{1}{\pi_1{}' s + 1}, \tag{41}$$

where $\pi_1{}'$ is the time constant of the filter. In order to ensure the estimation effect of $d_{\varphi_{ry}}$, the time constant $\pi_1{}'$ should be set small enough.

Similarly, according to equation (34), the error between the filter output and input is defined as

$$y_4{}' = x_{4d}{}' - x_{4c}{}'. \tag{42}$$

Combining equations (35), (42), and (33), we can obtain

$$x_4{}' = s_4{}' + x_{4d}{}' + \xi_4{}' = s_4{}' + y_4{}' + x_{4c}{}' + \xi_4{}' = s_4{}' + y_4{}' + \frac{-f_3{}' - k_3{}' s_3{}' - \widehat{d}_\alpha + \dot{x}_{3d}{}' - h_3{}'\xi_3{}' + \xi_4{}'}{g_3{}'} + \xi_4{}'. \tag{43}$$

Table 1: Initial state of missiles and the target.

Object	Position (m)	Velocity (m/s)	Acceleration (m/s^2)	Attack angle (°)	Elevator deflection (°)
Missile A	[020000]	200	0	1.0124	5.6
Missile B	[03000500]	250	0	0.8566	3.7
Missile C	[03000 − 500]	250	0	0.8566	3.7
Target	[500000]	/	/	/	/

Table 2: Desired impact LOS angle and attack angle of missiles.

Object	φ_{ry}^d (°)	φ_{rz}^d (°)	α^d (°)
Missile A	60	0	0.5
Missile B	90	0	0.5
Missile C	90	0	0.5

Table 3: Actual LOS angle, attack angle, and miss distance results at missile impact points.

Object	φ_{ry} (°)	φ_{rz} (°)	α (°)	Miss distance (m)
Missile A	59.07	0.10	0.48	0.0410
Missile B	86.77	0.32	0.56	0.0424
Missile C	87.42	-0.49	0.45	0.0451

Substituting equation (43) into (31), we get

$$\dot{s}_3{}' = -k_3{}' s_3{}' + g_3{}' s_4{}' + g_3{}' y_4{}' + g_3{}' \xi_4{}' - \widehat{d}_\alpha + d_\alpha. \quad (44)$$

Therefore, the observer designed in this section for estimating d_α is shown in Figure 3.

In Figure 3, the expression of low-pass filter $G_2{}'(s)$ is:

$$G_2{}'(s) = \frac{1}{\pi_2{}' s + 1} \quad (45)$$

where $\pi_2{}'$ is the time constant of the filter. In order to ensure the estimation effect of d_α, the time constant $\pi_2{}'$ should be set small enough.

Similarly, substituting equation (37) into (35), we can obtain

$$\dot{s}_4{}' = -k_4{}' s_4{}' - \widehat{d}_{\omega_z} + d_{\omega_z}. \quad (46)$$

Therefore, the observer designed in this section for estimating d_{ω_z} is shown in Figure 4.

In Figure 4, the expression of low-pass filter $G_3{}'(s)$ is

$$G_3{}'(s) = \frac{1}{\pi_3{}' s + 1}, \quad (47)$$

where $\pi_3{}'$ is the time constant of the filter. In order to ensure the estimation effect of d_{ω_z}, the time constant $\pi_3{}'$ should be set small enough.

To sum up, $\widehat{d}_{\varphi_{ry}}$, $\widehat{d}_\alpha$, and $\widehat{d}_{\omega_z}$ in equations (29), (33), and (37) are obtained by the disturbance observers shown in Figures 2–4, respectively.

The controller work steps are presented in Pseudocode 1.

3.3. Stability Analysis of the Proposed Robust IGC Control Method. The robust IGC control method is designed by using dynamic surface control and nonlinear disturbance observer; then, we analyze the stability of the IGC control method.

The estimation errors of the above three disturbance observers are defined as

$$\begin{aligned} e_1 &= d_{\varphi_{ry}} - \widehat{d}_{\varphi_{ry}}, \\ e_2 &= d_\alpha - \widehat{d}_\alpha, \\ e_3 &= d_{\omega_z} - \widehat{d}_{\omega_z}. \end{aligned} \quad (48)$$

Then, equations (40), (44), and (46) can be written as

$$\dot{s}_2{}' = -k_2{}' s_2{}' + g_2{}' s_3{}' + g_2{}' y_3{}' + g_2{}' \xi_3{}' + e_1, \quad (49)$$

$$\dot{s}_3{}' = -k_3{}' s_3{}' + g_3{}' s_4{}' + g_3{}' y_4{}' + g_3{}' \xi_4{}' + e_2, \quad (50)$$

$$\dot{s}_4{}' = -k_4{}' s_4{}' + e_3. \quad (51)$$

Taking the derivatives on both sides of equations (38) and (42), respectively, and combining equations (30) and (34), the following can be obtained:

$$\dot{y}_3{}' = -\frac{y_3{}'}{\tau_3{}'} + b_3{}', \quad (52)$$

$$\dot{y}_4{}' = -\frac{y_4{}'}{\tau_4{}'} + b_4{}', \quad (53)$$

where $b_i{}' = -\dot{x}_{ic}{}' (i = 3, 4)$ is a continuous function, and its boundedness can be obtained from Assumption 1. Therefore, it can be seen that $|b_i{}'| \le \eta_i{}' (i = 3, 4)$, where $\eta_i{}' (i = 3, 4)$ is the normal number.

The Lyapunov function is defined as

$$L = \frac{s_2{}'^2 + s_3{}'^2 + s_4{}'^2 + y_3{}'^2 + y_4{}'^2 + \xi_2{}'^2 + \xi_3{}'^2 + \xi_4{}'^2}{2}. \quad (54)$$

Taking the derivatives on both sides of equation (54) and

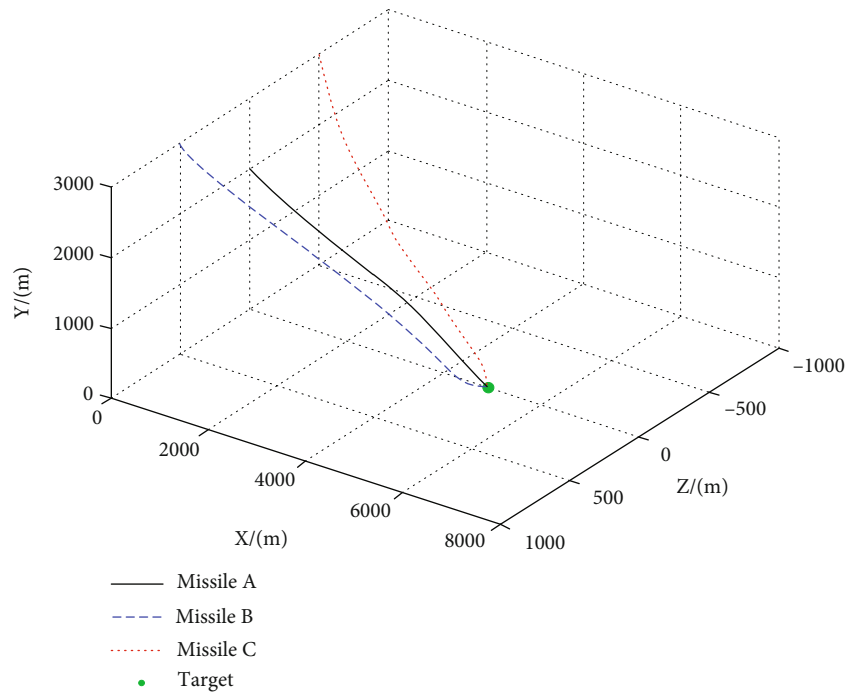

Figure 5: Three-dimensional trajectory of missiles A, B, and C and the target in angle penetration attack.

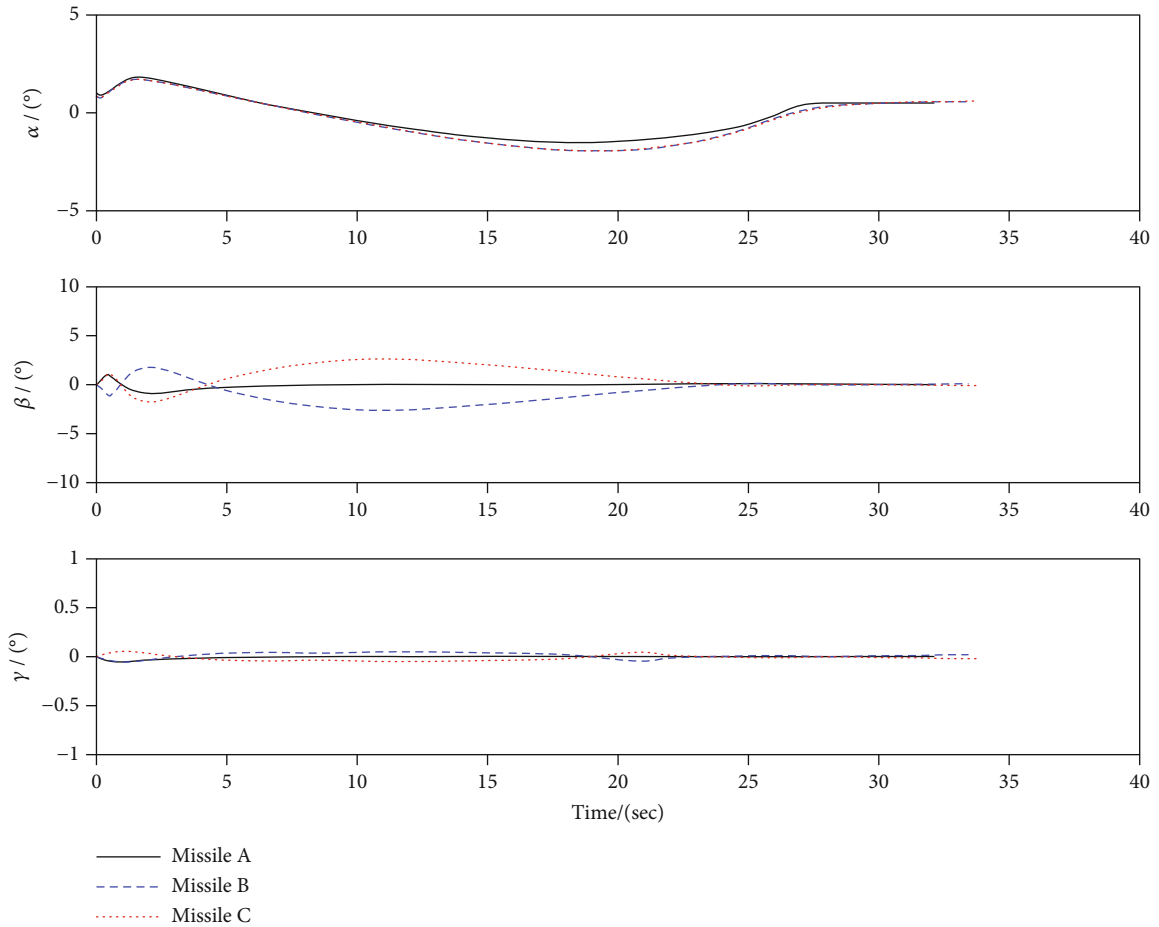

Figure 6: Response curves of the attack angle, sideslip angle, and roll angle of three missiles.

combining equations (49)–(53), the following can be obtained:

$$\begin{aligned}\dot{L} &= s_2'\left(-k_2's_2' + g_2's_3' + g_2'y_3' + g_2'\xi_3' + e_1\right)\\ &\quad + s_3'\left(-k_3's_3' + g_3's_4' + g_3'y_4' + g_3'\xi_4' + e_2\right)\\ &\quad + s_4'\left(-k_4's_4' + e_3\right) + y_3'\left(-\frac{y_3'}{\tau_3'} + b_3'\right)\\ &\quad + y_4'\left(-\frac{y_4'}{\tau_4'} + b_4'\right) + \xi_2'\left(-h_2'\xi_2' + \xi_3'\right)\\ &\quad + \xi_3'\left(-h_3'\xi_3' + \xi_3\right) + \xi_3(-h_3\xi_3 + g_3\Delta\delta_z)\\ &= -k_2's_2'^2 - k_3's_3'^2 - k_4's_4'^2 - \frac{y_3'^2}{\tau_3'} - \frac{y_4'^2}{\tau_4'} - h_2'\xi_2'^2\\ &\quad - h_3'\xi_3'^2 - h_4'\xi_4'^2 + g_2's_2's_3' + g_2's_2'y_3' + g_2's_2'\xi_3'\\ &\quad + s_2'e_1 + g_3's_3's_4' + g_3's_3'y_4' + g_3's_3'\xi_4' + s_3'e_2\\ &\quad + s_4'e_3 + y_3'b_3' + y_4'b_4' + \xi_2'\xi_3' + \xi_3'\xi_4' + g_2'\xi_3'\Delta\delta_z.\end{aligned} \tag{55}$$

According to Young's inequality and $|b_i'| \le \eta_i'(i = 3, 4)$, it can be deduced that

$$\begin{aligned}\dot{L} &\le -k_2's_2'^2 - k_3's_3'^2 - k_4's_4'^2 - \frac{y_3'^2}{\tau_3'} - \frac{y_4'^2}{\tau_4'} - h_2'\xi_2'^2\\ &\quad - h_3'\xi_3'^2 - h_4'\xi_4'^2 + \frac{g_2'^2s_2'^2}{4} + s_3'^2 + \frac{g_2'^2s_2'^2}{4} + y_3'^2\\ &\quad + \frac{g_2'^2s_2'^2}{4} + \xi_3'^2 + s_2'^2 + \frac{e_1^2}{4} + \frac{g_3'^2s_3'^2}{4} + s_4'^2\\ &\quad + \frac{g_3'^2s_3'^2}{4} + y_4'^2 + \frac{g_3'^2s_3'^2}{4} + \xi_4'^2 + s_3'^2 + \frac{e_2^2}{4} + s_4'^2\\ &\quad + \frac{e_3^2}{4} + y_3'^2 + \frac{b_3'^2}{4} + y_4'^2 + \frac{b_4'^2}{4} + \frac{\xi_2'^2}{2} + \frac{\xi_3'^2}{2}\\ &\quad + \frac{\xi_3'^2}{2} + \frac{\xi_4'^2}{2} + \frac{\xi_4'^2}{2} + \frac{\left(g_4'\Delta\delta_z\right)^2}{2}.\end{aligned} \tag{56}$$

Further, the following inequality holds:

$$\begin{aligned}\dot{L} &\le -\left(k_2' - \frac{3g_2'^2}{4} - 1\right)s_2'^2 - \left(k_3' - \frac{3g_3'^2}{4} - 2\right)s_3'^2\\ &\quad - \left(k_4' - 2\right)s_4'^2 - \left(h_2' - 0.5\right)\xi_2'^2 - \left(h_3' - 2\right)\xi_3'^2\\ &\quad - \left(h_4' - 2\right)\xi_4'^2 - \left(\frac{1}{\tau_3'} - 2\right)y_3'^2 - \left(\frac{1}{\tau_4'} - 2\right)y_4'^2\\ &\quad + \frac{e_1^2 + e_2^2 + e_3^2}{4} + \frac{\eta_3'^2 + \eta_4'^2}{4} + \frac{g_4'^2\Delta\delta_z^2}{2}.\end{aligned} \tag{57}$$

If the parameters $k_i'(i = 2, 3, 4)$ and $\tau_i'(i = 3, 4)$ to be set meet the following inequalities,

$$\begin{cases} k_2' - \dfrac{3g_2'^2}{4} - 1 \ge \dfrac{\varsigma}{2}, k_3' - \dfrac{3g_3'^2}{4} - 2 \ge \dfrac{\varsigma}{2}, k_4' - 2 \ge \dfrac{\varsigma}{2},\\ h_2' - 0.5 \ge \dfrac{\varsigma}{2}, h_3' - 2 \ge \dfrac{\varsigma}{2}, h_4' - 2 \ge \dfrac{\varsigma}{2},\\ \dfrac{1}{\tau_3'} - 2 \ge \dfrac{\varsigma}{2}, \dfrac{1}{\tau_4'} - 2 \ge \dfrac{\varsigma}{2}, \end{cases} \tag{58}$$

where ς is the normal number.

Combining equations (57) and (58), we can obtain

$$\dot{L} \le \zeta - \varsigma L, \tag{59}$$

where $\zeta = (\eta_3'^2 + \eta_4'^2 + e_1^2 + e_2^2 + e_3^2/4) + (g_4'^2\Delta\delta_z^2/2)$..

From equation (59), we can get

$$\lim_{t\longrightarrow\infty} L \le \frac{\zeta}{\varsigma}. \tag{60}$$

Assuming that the designed disturbance observer can better estimate the uncertainty, it can be seen that

$$\lim_{t\longrightarrow\infty} e_i = 0, \quad i = 1, 2, 3. \tag{61}$$

In the later flight stage of missiles attacking the target, it can be assumed that there is no input saturation; that is, when $t \longrightarrow \infty$, $\Delta\delta_z = 0$ holds. At this time, equation (60) becomes

$$\lim_{t\longrightarrow\infty} L \le \frac{\eta_2^2 + \eta_3^2}{4\varsigma}. \tag{62}$$

From equation (62), it can be seen that the upper bound of L depends on $\eta_i'(i = 3, 4)$ and ς. If ς is large enough, L can become arbitrarily small, and s_2', s_3', s_4' and y_3', y_4' are ultimately uniformly bounded.

Since $x_1' = 0$ is one of the control objectives, in order to analyze its transient tracking error, we define

$$L_\xi = \frac{\xi_2'^2 + \xi_3'^2 + \xi_4'^2}{2}. \tag{63}$$

By taking the derivatives on both sides of equation (63), according to Young's inequality, the following can be obtained:

$$\begin{aligned}\dot{L}_\xi &= \sum_{i=2}^{4}\xi_i'\dot{\xi}_i' = -h_2'\xi_2'^2 + \xi_2'\xi_3' - h_3'\xi_3'^2 + \xi_3'\xi_4'\\ &\quad - h_4'\xi_4'^2 + g_4'\xi_4'\Delta\delta_z \le -\left(h_2' - 0.5\right)\xi_2'^2\\ &\quad - \left(h_3' - 1\right)\xi_3'^2 - \left(h_4' - 2\right)\xi_4'^2 + \frac{g_4'^2\Delta\delta_z^2}{2}.\end{aligned} \tag{64}$$

Let $h = \min(h_2' - 0.5, h_3' - 1, h_4' - 2)$; then, equation (64) becomes

$$\dot{L}_\xi \le -h\left(\xi_1^2 + \xi_2^2 + \xi_3^2\right) + \frac{g_3^2 \Delta\delta_z^2}{2}. \tag{65}$$

Taking the derivatives on both sides of equation (65) within $[0, \infty]$, we can obtain

$$L_\xi(\infty) - L_\xi(0) \le -h\int_0^\infty \left(\xi_2'^2 + \xi_3'^2 + \xi_4'^2\right)dt + \frac{1}{2}\int_0^\infty \left(g_4'^2 \Delta\delta_z^2\right)dt. \tag{66}$$

According to equation (66), the following inequality can be obtained:

$$\begin{aligned}\left\|\xi_2'\right\|_2^2 &\le -\int_0^\infty \left(\xi_3'^2 + \xi_4'^2\right)dt + \frac{\left(1/2\int_0^\infty \left(g_4'^2 \Delta\delta_z^2\right)dt - L_\xi(\infty) + L_\xi(0)\right)}{h} \\ &\le \frac{\left(1/2\int_0^\infty \left(g_4'^2 \Delta\delta_z^2\right)dt + L_\xi(0)\right)}{h} = \frac{\left\|g_4' \Delta\delta_z\right\|_2^2}{2h} + \frac{L_\xi(0)}{h}.\end{aligned} \tag{67}$$

Then, the upper bound of $\left\|\xi_2'\right\|_2$ can be expressed as

$$\left\|\xi_2'\right\|_2 \le \frac{\left\|g_4' \Delta\delta_z\right\|_2}{\sqrt{2h}} + \frac{\sqrt{L_\xi(0)}}{\sqrt{h}}. \tag{68}$$

Similarly, taking the derivatives on both sides of equation (59) within $[0, \infty]$, we can obtain

$$\begin{aligned}L(\infty) - L(0) \le &-\varsigma\int_0^\infty \left(s_2'^2 + s_3'^2 + s_4'^2 + L_\xi + y_3'^2 + y_4'\right)dt \\ &+ \frac{1}{2}\int_0^\infty \left(g_4'^2 \Delta\delta_z^2\right)dt + \frac{1}{4}\int_0^\infty \left(\eta_3'^2 + \eta_4'^2 + s_2'^2 + s_3'^2 + s_4'^2\right)dt.\end{aligned} \tag{69}$$

According to equation (69), the following inequality can be obtained:

$$\begin{aligned}\left\|s_2'\right\|_2^2 \le &-\int_0^\infty \left(s_3'^2 + s_4'^2 + L_\xi + y_3'^2 + y_4'^2\right)dt \\ &+ \frac{\left(1/2\int_0^\infty \left(g_4'^2 \Delta\delta_z^2\right)dt - L(\infty) + L(0)\right)}{\varsigma} \\ &+ \frac{1}{4\varsigma}\int_0^\infty \left(\eta_3'^2 + \eta_4'^2 + e_1^2 + e_2^2 + e_3^2\right)dt \\ \le &\frac{\left\|\eta_3'\right\|_2^2 + \left\|\eta_4'\right\|_2^2 + \left\|e_1\right\|_2^2 + \left\|e_2\right\|_2^2 + \left\|e_3\right\|_2^2}{4\varsigma} \\ &+ \frac{\left\|g_4' \Delta\delta_z\right\|_2^2}{2\varsigma} + \frac{L(0)}{\varsigma} \\ \le &\frac{\left(\left(\left\|\eta_3'\right\|_2 + \left\|\eta_4'\right\|_2 + \left\|e_1\right\|_2 + \left\|e_2\right\|_2 + \left\|e_3\right\|_2\right)/2 + \left\|g_4' \Delta\delta_z\right\|_2/\sqrt{2}\right)^2}{\varsigma} \\ &+ \frac{L(0)}{\varsigma}.\end{aligned} \tag{70}$$

Therefore, the following can be obtained:

$$\begin{aligned}\left\|x_1' - \xi_2'\right\|_2 &= \left\|s_2'\right\|_2 \\ &\le \frac{\left(\left(\left\|\eta_3'\right\|_2 + \left\|\eta_4'\right\|_2 + \left\|e_1\right\|_2 + \left\|e_2\right\|_2 + \left\|e_3\right\|_2\right)/2 + \left\|g_4' \Delta\delta_z\right\|_2/\sqrt{2} + \sqrt{L(0)}\right)}{\sqrt{\varsigma}}.\end{aligned} \tag{71}$$

Combining equations (68) and (71) and making $\xi_i'(0) = 0, (i = 2, 3, 4)$ so that $L_\xi(0) = 0$, we get

$$\begin{aligned}\left\|x_1'\right\|_2 \le &\frac{\left\|\eta_3'\right\|_2 + \left\|\eta_4'\right\|_2 + \left\|e_1\right\|_2 + \left\|e_2\right\|_2 + \left\|e_3\right\|_2}{2\sqrt{\varsigma}} \\ &+ \frac{\left\|g_4' \Delta\delta_z\right\|_2}{\sqrt{2\varsigma}} + \frac{\left\|g_4' \Delta\delta_z\right\|_2}{\sqrt{2h}}.\end{aligned} \tag{72}$$

Equation (72) gives the explicit expression of the transient tracking error of the desired line-of-sight angle in the longitudinal plane.

According to equations (62) and (72), the following conclusions can be drawn.

Conclusion 2. For the decoupling IGC nonlinear system model of angle penetration attack shown in equation (20) satisfying Assumption 1, the uncertain performance in the system model is effectively estimated by the disturbance observers shown in Figures 2–4. When the dynamic surface (DSC) control method shown in equation (37) is established, and all states s_1', s_2', s_3', s_4' and y_2', y_3', y_4' of the closed-loop system will be ultimately uniformly bounded by setting appropriate parameters. Meanwhile, by increasing the parameter $k_1', k_2', k_3', k_4', h_1', h_2', h_3', h_4'$ and decreasing the parameter $\tau_2', \tau_3', \tau_4'$, the above states will be arbitrarily small. In conclusion, the proposed cooperative IGC design method is stable.

Note 3. In this section, an IGC design method based on the adaptive dynamic surface and nonlinear disturbance observer is designed for the subsystem model of the IGC pitch channel of the missile in the longitudinal plane. For the subsystem model of the IGC yaw channel and roll channel shown in equations (16) and (17), respectively, which contain unknown uncertainties and have input constraints on control inputs δ_z, δ_y and δ_x, the control goal of the yaw channel is to design the controller to make the terminal line-of-sight angle of missile and target meet the requirements of desired impact angle and to ensure that the line-of-sight rate tends to zero and to meet the requirements of low miss distance. The control goal of the roll channel is to minimize the rolling. The controller design still adopts the IGC design method of the adaptive dynamic surface and disturbance observer proposed in this section.

4. Simulation and Analysis

In order to verify the effectiveness and practicability of the IGC design method based on adaptive dynamic surface for

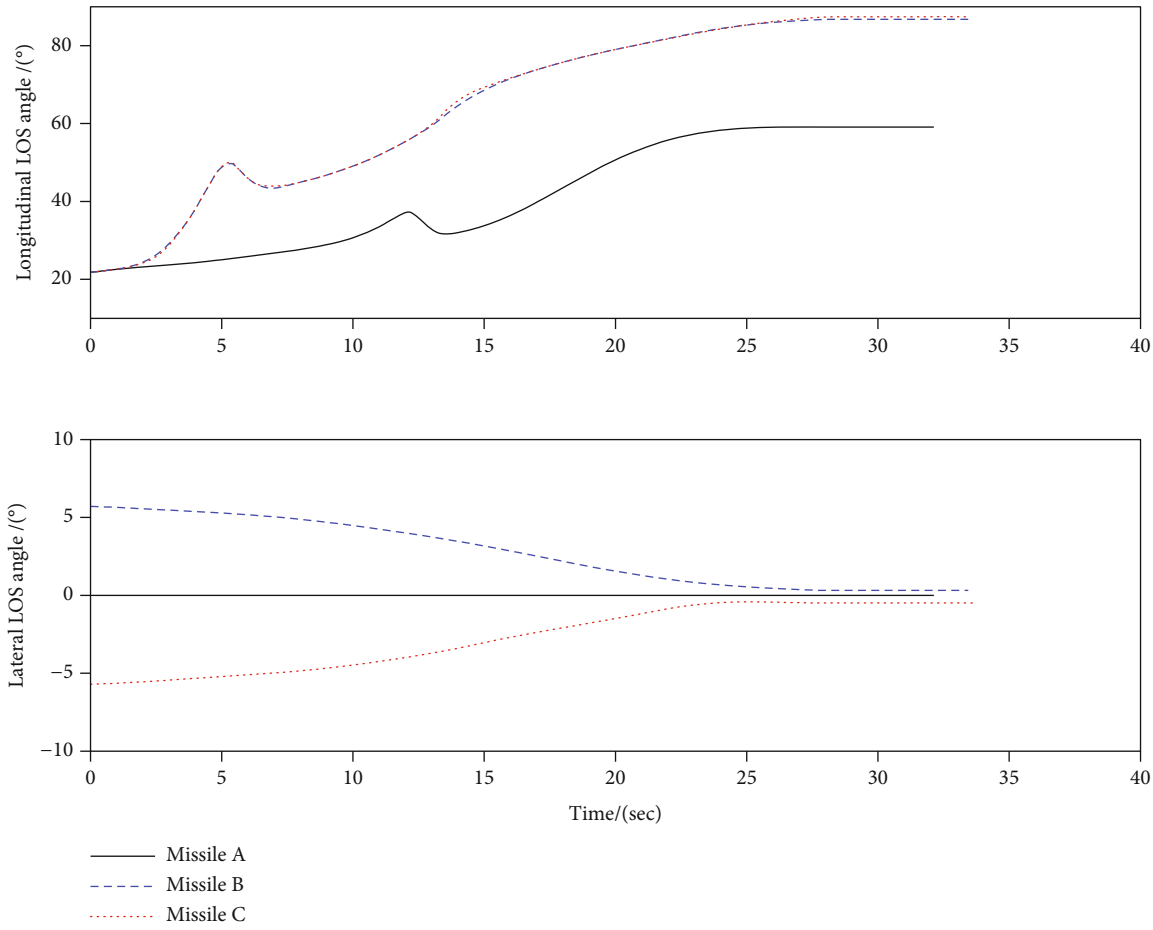

Figure 7: LOS angle curves in the longitudinal plane and lateral plane of three missiles.

multimissiles cooperative attack on battlefield targets, the computer simulation experiments of multimissile angle penetration attack mission are carried out. During the experiment, all simulations use MATLAB R2021a software, and the PC parameters used are Intel i7, 4-Core, 2.40 GHz, 64 bit, and 8 GB RAM.

The simulation scenario is set as that three missiles (missiles A, B, and C) perform the task of attacking ground stationary targets. The initial state and relevant control parameters of each missile and target are set in Table 1.

Except that the initial pitch angle is equal to the attack angle, the attitude angle and angle rate of three missiles are zero, and the initial aileron deflection angle and rudder deflection angle are also zero. Generally, the velocity and mass of three missiles can be regarded as invariants in the whole attack process. There is a fixed perturbation deviation +20% in the aerodynamic parameters of missiles and +20% fixed noise interference in the measurement. The input limits of elevator deflection angle, rudder deflection angle, and aileron deflection angle are ±10°, ±10°, and ±10°, respectively.

The desired terminal impact angle constraints set in the simulation are shown in Table 2. $\varphi_{ry}^{d}, \varphi_{rz}^{d}$ represent the desired impact LOS angle of missiles in the longitudinal plane and lateral plane, respectively; α^{d} is the desired impact attack angle of missiles.

In equation (35), the parameter $h_i{}'$ of the auxiliary subsystem is set as $h_i{}' = 2.5$, $(i = 1, 2, 3, 4)$, respectively; in equations (25), (29), (33), and (37), the virtual control parameters of the dynamic surface are set as $k_i{}' = 2.5$, $(i = 1, 2, 3, 4)$, respectively; in equations (26), (30), and (34), the filtering time constants of the first-order filter are, respectively, set as $\tau_i{}' = 0.2\text{s}(i = 2, 3, 4)$; in equations (41), (45), and (47), the filtering time constants of the disturbance observer are, respectively, set as $\pi_i{}' = 0.004\text{s}(i = 1, 2, 3)$.

Table 3 shows the actual impact angle and miss distance of missiles A, B, and C. The curves shown in Figure 5 are the three-dimensional motion trajectories of three missiles and targets, respectively, and three groups of curves shown in Figure 6 are the changes of attack angle, sideslip angle, and roll angle of three missiles, respectively. Two groups of curves shown in Figure 7 represent the change of actual LOS angle in the longitudinal plane and lateral plane of three missiles, respectively, and two groups of curves shown in Figure 8 are the change of LOS angle rate in the longitudinal plane and lateral plane of three missiles, respectively.

According to the simulation results in Table 3 and Figure 5, missiles A, B, and C can intercept the target with

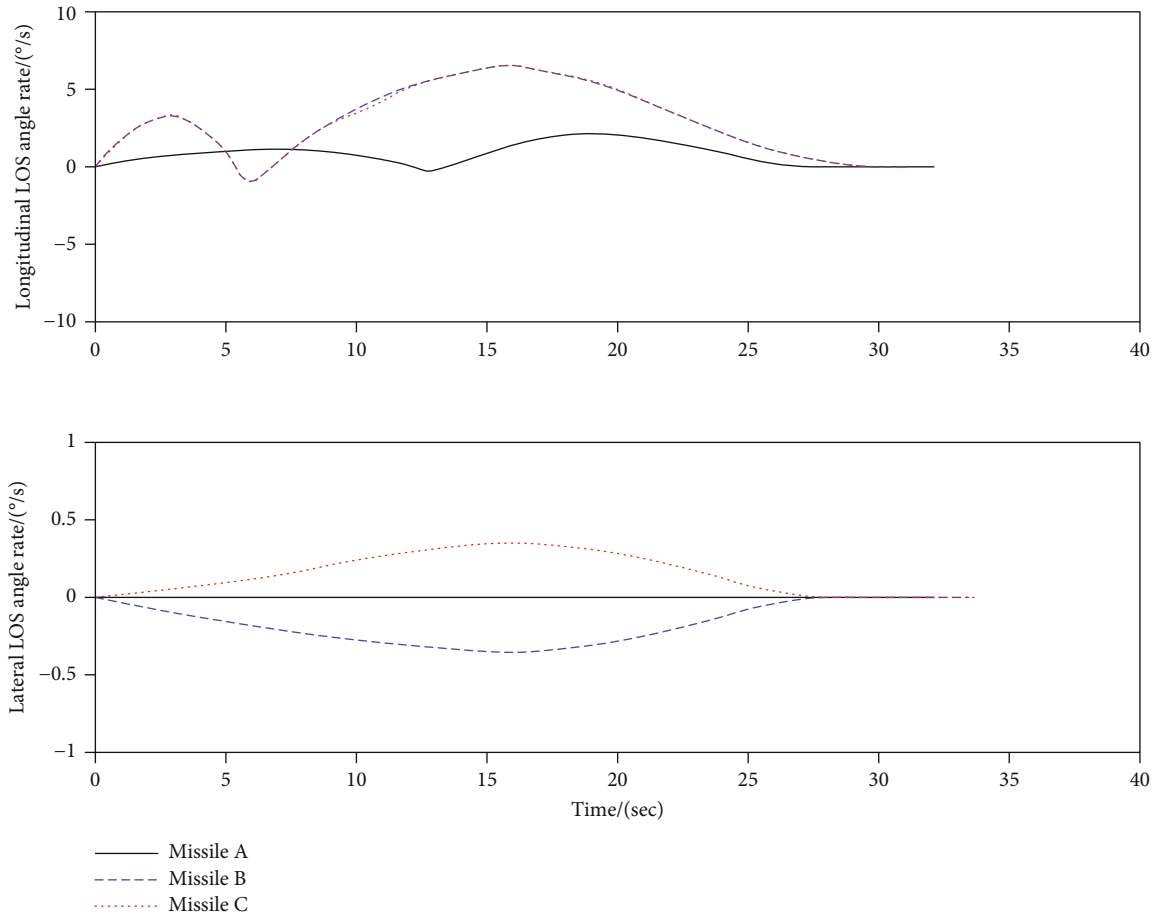

Figure 8: LOS angle rate curves in the longitudinal plane and lateral plane of three missiles.

Table 4: Performance comparison of three algorithms.

Algorithm	Mean miss distance (m)			φ_{ry} (°)		
	Missile A	Missile B	Missile C	Missile A	Missile B	Missile C
Traditional method	1.7322	1.8106	1.8545	45.82	62.19	66.56
SMC method	1.0057	1.0213	1.0388	62.11	84.54	85.71
Proposed method	0.0416	0.0429	0.0462	59.12	86.94	87.63

a small miss distance to achieve accurate attack on the target. Among them, the actual terminal LOS angle in the longitudinal plane of missile A is 59.07°, which differs little from the desired impact angle constraint 60°. The actual terminal LOS angle in the longitudinal plane of missiles B and C are 87.42° and 87.42°, respectively, which is equivalent to reaching the desired impact angle constraint 90° and means that the vertical attack on the target is realized.

According to the simulation results in Figures 5–8, while meeting the constraints of terminal line-of-sight angle, the three missiles can also ensure that each missile can complete the target attack at a sufficiently small attack angle, and the impact attack angles of missiles A, B, and C are 0.48°, 0.56° and 0.45°, respectively, which meets the requirements of angle penetration attack. At the same time, the three missiles maintain a relatively gentle flight state during the flight, which can ensure that the angle rate changes of missiles A, B, and C are maintained in a small range and bear small overload changes.

To compare with existing methods, such as the traditional guidance and control method (traditional method) [12] and sliding mode control method (SMC method) [15], Monte Carlo simulation is used to conduct 100 robustness experiments in the same simulation conditions. The mean miss distance and LOS angle are shown in Table 4.

According to the simulation results in Table 4, missiles A, B, and C can attack the target with small mean miss distance; meanwhile, they can meet with the desired impact angle requirements by using the proposed method in this paper. Both the traditional method and SMC method make big mean miss distance compared with the proposed method. The SMC method can meet with the desired impact

angle requirements, while the traditional method has big error in the desired impact angle. The reason is that the traditional method separates the guidance and control system, which will make a bad impact on the control accuracy and coordination performance. And the SMC method can achieve coordination control with the nonlinear control ability, but it cannot deal with the unknown uncertainty which will deduce some control errors.

5. Conclusions

This paper mainly studies the integrated guidance and control (IGC) design method for multimissile angle penetration attack. According to the requirements of multimissile angle penetration attack, the IGC system model with impact angle constraint is established. Considering the dynamic constraints, nonlinear input saturation, terminal line-of-sight, and attack angle constraints, a robust IGC control method for angle penetration attack is designed based on the adaptive dynamic surface and nonlinear disturbance observer, and the stability of the IGC design method is proven by the Lyapunov theorem. The simulation results show that the method proposed in this paper can not only ensure the accurate attack of each missile on the target but also ensure the coordination of multimissile flight states, meet the terminal impact angle requirement of each missile, and finally realize the multimissile angle penetration attack mission. The paper makes a contribution to the cooperative integrated guidance and control system design, and the research results will benefit practical missions of high-speed UAVs and missiles in the future. The processing of nonlinear uncertainties such as hysteresis and dead time in the control system is the focus of the next research.

Data Availability

The data used to support the findings of this study are included within the article.

Conflicts of Interest

The authors declare no conflict of interest.

Acknowledgments

The authors acknowledge the funding received from the following science foundations: the National Natural Science Foundation of China (Nos. 62101590 and 62176214) and the Natural Science Foundation of Shaanxi Province, China (2020JQ-481, 2019JQ-014).

References

[1] H. Yu, K. Dai, H. Li et al., "Distributed cooperative guidance law for multiple missiles with input delay and topology switching," *Journal of Franklin Institute*, vol. 358, no. 17, pp. 9061–9085, 2021.

[2] P. Zhang and X. Zhang, "Multiple missiles fixed-time cooperative guidance without measuring radial velocity for maneuvering targets interception," *ISA Transations*, 2021, In Press, Available online 17 July 2021.

[3] J. Yu, X. Dong, Q. Li, and Z. Ren, "Cooperative integrated practical time-varying formation tracking and control for multiple missiles system," *Aerospace Science and Technology*, vol. 93, article 105300, 2019.

[4] K. Chen, "Full state constrained stochastic adaptive integrated guidance and control for STT missiles with non-affine aerodynamic characteristics," *Information Sciences*, vol. 529, pp. 42–58, 2020.

[5] I. S. Jeon, J. I. Lee, and M. J. Tahk, "Impact-time-control guidance law for anti-ship missiles," *IEEE Transactitons on Control System Technology*, vol. 14, no. 2, pp. 260–266, 2006.

[6] S. R. Kumar and D. Ghose, "Sliding mode control based guidance law with impact time constrains," in *2013 American Control Conference*, pp. 5760–5765, Washington, DC, USA, June 2013.

[7] I. S. Jeon, J. I. Lee, and M. J. Tahk, "Homing guidance law for cooperative attack of multiple missiles," *Journal of Guidance, Control and Dynamics*, vol. 33, no. 1, pp. 275–280, 2010.

[8] Y. Wang, S. Fan, J. Wang, and G. Wu, "Quick identification of guidance law for an incoming missile using multiple-model mechanism," *Chinese Journal of Aeronautics*, 2021, In Press, Available online 24 November 2021.

[9] N. Harl and S. N. Balakrishnan, "Impact time and angle guidance with sliding mode control," *IEEE Transactions on Control System and Technology*, vol. 20, no. 6, pp. 1436–1449, 2012.

[10] B. Jung and Y. Kim, "Guidance laws for anti-ship missiles using impact angle and impact time," in *AIAA Guidance, Navigation, and Control Conference and Exhibit*, pp. 1–13, Keystone, Colorado, USA, August 2006.

[11] M. Hou, X. Liang, and G. Duan, "Adaptive block dynamic surface control for integrated missile guidance and autopilot," *Chinese Journal of Aeronautics*, vol. 26, no. 3, pp. 741–750, 2013.

[12] C. Ming, X. Wang, and R. Sun, "A novel non-singular terminal sliding mode control-based integrated missile guidance and control with impact angle constraint," *Aerospace Science and Technology*, vol. 94, article 105368, 2019.

[13] J. Zhao and S. Yang, "Integrated cooperative guidance framework and cooperative guidance law for multi-missile," *Chinese Journal of Aeronautics*, vol. 31, no. 3, pp. 546–555, 2018.

[14] X. Shao and H. Wang, "Back-stepping active disturbance rejection control design for integrated missile guidance and control system via reduced-order ESO," *ISA Transacitons*, vol. 57, pp. 10–22, 2015.

[15] T. Shima, M. Idan, and O. M. Golan, "Sliding-mode control for integrated missile autopilot guidance," *Journal of Guidance, Control and Dynamics*, vol. 29, no. 2, pp. 250–260, 2006.

[16] X. Shao and H. Wang, "Active disturbance rejection based trajectory linearization control for hypersonic reentry vehicle with bounded uncertainties," *ISA Transactions*, vol. 54, pp. 27–38, 2015.

[17] D. Swaroop, J. K. Hedrick, P. P. Yip, and J. C. Gerdes, "Dynamic surface control for a class of nonlinear systems," *IEEE Transactions on Automatic Control*, vol. 45, no. 10, pp. 1893–1899, 2000.

[18] W. Bu and Q. Qi, "Fuzzy optimal tracking control of hypersonic flight vehicles via single-network adaptive critic design," *IEEE Transactions on Fuzzy Systems*, vol. 30, no. 1, pp. 270–278, 2022.

[19] Z. Peng, Y. Jiang, and J. Wang, "Event-triggered dynamic surface control of an underactuated autonomous surface vehicle for target enclosing," *IEEE Transactions on Industrial Electronics*, vol. 68, no. 4, pp. 3402–3412, 2021.

[20] X. Bu, Q. Qi, and B. Jiang, "A simplified finite-Time fuzzy neural controller with prescribed performance applied to waverider aircraft," *IEEE Transactions on Fuzzy systems*, vol. 99, pp. 1–9, 2021.

[21] H. Zhou, H. Zhao, H. Huang, and X. Zhao, "Integrated guidance and control design of the suicide UCAV for terminal attack," *Journal of Systems Engineering and Electronics*, vol. 28, no. 3, pp. 546–555, 2017.

[22] H. Huang, X. Zhao, and X. Zhang, "Intelligent guidance and control methods for missile swarm," *Computational Intelligence and Neuroscience*, vol. 2022, Article ID 8235148, 9 pages, 2022.